2025
12(3), 1271

Chemical Biology
LETTERS

Synthesis and in-vitro anti-EGFR screening of new 1,2,3-triazole-benzimidazole hybrids and in-silico studies

Advaitha Vanaparthy[1], Kranthi Kumar Thallapally[2], Devendar Banothu[3], Krishnakumar Polkampally[4], Raja Shekhar Kondrapolu[5], Satheesh Kumar Nukala[6]*, Ravinder Manchal[1]*

[1] Department of Chemistry, Chaitanya (Deemed to be University), Hyderabad, 500075 India. [2]Department of Chemistry, Sreenidhi Institute of Science and Technology, Hyderabad, 501301 India. [3]Department of Chemistry, Kakatiya University, Warangal, Telangana, 506009 India. [4]Department of Chemistry, Osmania University, Hyderabad, Telangana, 500007 India. [5]Department of Chemistry, University of Arkansas at Little Rock, 2801 South University Avenue Little Rock, AR 72204, USA. [6]Government Junior College, Mustabad, Rajanna Sircilla, Telangana, 505404 India.

Submitted on: 28-Jan-2025, Accepted and Published on: 04-Apr-2025

Article

ABSTRACT

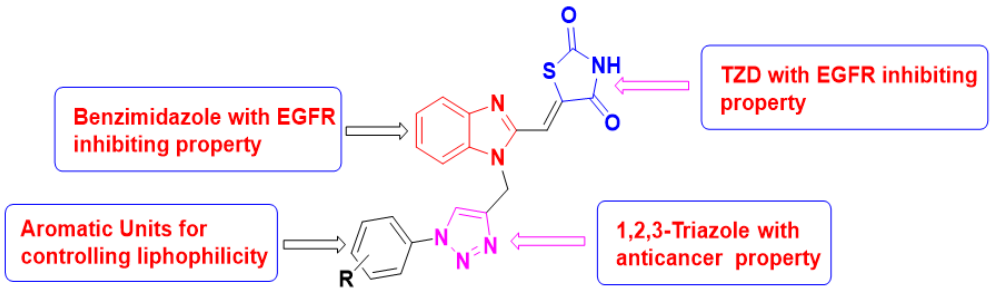

Herein, the synthesis of benzimidazole- thiazolidine-2,4-dione -1,2,3-triazole conjugates (**7a-7n**) using copper (I) catalysed azide alkyne cycloaddition is reported. The synthesized compounds were screened for in vitro anticancer activity against MCF-7, MDA-MB-468 and MDA-MB-231 human breast cancer cells. Among all the compounds, four compounds namely **7d**, **7i**, **7k**, and **7n** displayed superior activity than 5-fluorouracil towards three breast cancer cell lines with IC_{50} values ranging from 1.8 µM to 9.7 µM. In vitro tyrosine kinase EGFR inhibition assay revealed that the compound **7d** have 2.8 times more potency than that of erlotinib with IC_{50} value of 0.15µM and remaining three compounds (**7i**, **7k** and **7n**) also have more activity than erlotinib. Molecular docking studies on EGFR protein indicated that compound **7d** exhibit greatest binding energy i.e. -11.04 kcal/mol compared to erlotinib. The molecule **7d** was characterized by using density functional theory (DFT) with B3LYP/6–311++ G (d, p) basis set. The structural parameters were obtained from geometry optimization. Finally in silico pharmacokinetic profile also determined where **7d** and **7i** followed all the rules like Lipinski rule, Ghose rule, Veber rule, Egan rule and Muegge rule without any deviation.

Keywords: Benzimidazole, Thiazolidine-2,4-dione, 1,2,3-triazole, EGFR, Docking, DFT and ADMET

INTRODUCTION

It is alarming to realize that nearly 20 million people around the world are diagnosed with cancer each year, leading to the devastation of millions of lives. The number of new cancer cases is on the rise globally, and if this trend continues, it could reach 30 million by 2040.[1] Currently, countries are largely relying on chemotherapy, which uses non-selective agents that can cause a range of serious side effects, including gastrointestinal, skin, hair follicle, and hematological toxicity. These effects can extend to the cardiac, nervous, hepatic, urinary, and pulmonary systems.[2,3] Therefore, the search for novel and selective anticancer agents is of utmost importance to mitigate the toxic effects associated with existing treatments.[4] In this context, protein tyrosine kinases are regarded as crucial targets because they play key roles in signal transduction pathways related to angiogenesis, proliferation, differentiation, and migration.[5,6] The epidermal growth factor receptor (EGFR) is a membrane receptor tyrosine kinase that is often overexpressed in various tumors. Inhibiting EGFR can lead to tumor suppression, as its signaling pathways are closely associated with tumor progression.[7-9]

The benzimidazole pharmacophore has been widely employed as a key structural element in the creation of numerous drugs with various therapeutic uses.[10] The biological activity of compounds featuring the benzimidazole unit arises from the interaction of the benzene and imidazole rings with various biologically relevant targets through non-covalent interactions.[11] Additionally, several benzimidazole-based anticancer candidates have been identified as effective EGFR inhibitors.[12] Notably, the third-generation

*Corresponding Authors: Prof Ravinder Manchal
Department of Chemistry, Chaitanya (Deemed to be University), Hyderabad, 500075 India, Email: ravinder@chaitanya.edu.in

Dr Satheesh Kumar Nukala, Government Junior College, Mustabad, Rajanna Sircilla, Telangana, 505404 India, Email: satheeshkumar.n.9@gmail.com,

URN:NBN:sciencein.cbl.2025.v12.1271
DOI:10.62110/sciencein.cbl.2025.v12.1271

https://pubs.thesciencein.org/cbl

EGFR inhibitor Nazartinib features a benzimidazole structure, while the other two candidates, Avitinib and Osimertinib, are derivatives of indolopyrimidine and indole, respectively, which act as bioisosteres of the benzimidazole ring.[13]

An extensive review of the literature shows that thiazolidine-2,4-dione (TZD) and rhodanine derivatives are considered valuable frameworks in drug design and discovery. Numerous TZD-containing compounds have been developed as potential anti-cancer agents.[14-16] For example B.B.V. Sailaja et. al[17] have developed benzimidazole-thiazolidine-2,4-dione-1,2,4-oxadiazole conjugates where one of the compound (**A;**) has shown EGFR inhibition with IC_{50} value of 0.26 micromolar and S. K. Koppula et. al.[18] have reported hybrid molecules containing 4-azaindole, TZD and 1,2,3-triazole pharmacophores where three compounds (**B**) have shown more EGFR inhibition potency than erlotinib.

Additionally, nitrogen-containing heterocyclic compounds with a triazole core are crucial in medicinal and pharmaceutical research due to their biological activity.[19] In particular, 1,2,3-triazole derivatives serve as valuable scaffolds, demonstrating a wide range of biological activities, including antimicrobial, antifungal, antitubercular, anti-inflammatory, anticancer, analgesic, anticonvulsant, and antityrosinase effects.[20-26] To be specific many reports available stating that 1,2,3-triazole as EGFR inhibitors. [27-31] Considering the medicinal applications of benzimidazole, thiazolodine-2,4-dione and 1,2,3-triazole mentioned above, we have designed compounds (**Figure 1**) incorporating three pharmacophores. This design is based on the benefits of the pharmacophore hybridization strategy. [32,33]

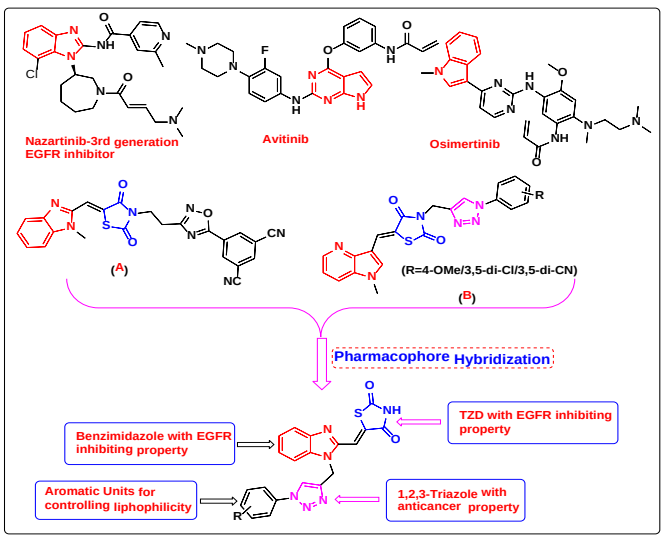

Figure 1: Designed strategy for the synthesis of benzimidazole-thiazolidine-2,4-dione -1,2,3-triazole conjugates

Results and Discussion

Chemistry

The entire synthesis of anticipated benzimidazole-thiazolidine-2,4-dione-1,2,3-triazole hybrids (**7a–7n**) was outlined in **scheme 1**. At the outset, 1*H*-benzo[*d*]imidazole-2-carbaldehyde (**1**) subjected to N-alkylation using 3-bromoprop-1-yne (**2**) by means of K_2CO_3 in DMF at RT for 4 h to yield 1-(prop-2-yn-1-yl)-1*H*-benzo[*d*]imidazole-2-carbaldehyde (**3**). The next step involves the synthesis of (*Z*)-5-((1-(prop-2-yn-1-yl)-1*H*-benzo[*d*]imidazol-2-yl)methylene)thiazolidine-2,4-dione (**5**) *via* Knoevenagel condensation of intermediate **3** with thiazolidine-2,4-dione (**4**) promoted by piperidine in EtOH at reflux temperature for 24 h. Finally, the [3+2] cycloaddition reaction of intermediate **5** with various aryl azides (**6a–6n**) under CuI catalysis led to give regioselective benzimidazole-thiazolidine-2,4-dione-1,2,3-triazole **(7a–7n)** in moderate to good yields.

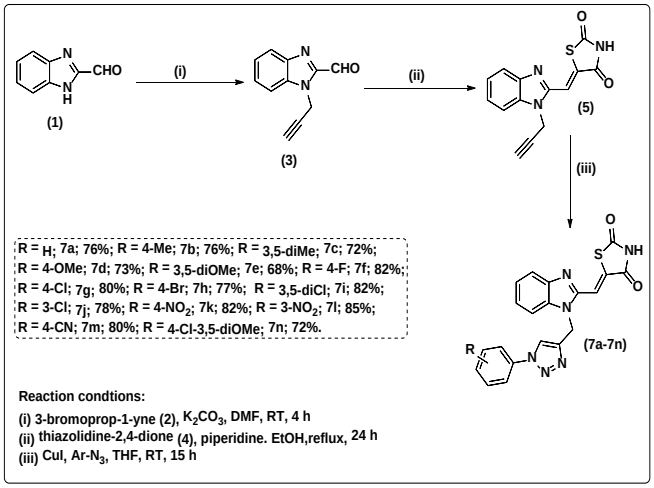

Scheme 1: Synthesis of benzimidazole- thiazolidine-2,4-dione -1,2,3-triazole conjugates (**7a-7n**)

In vitro anticancer activity

All the newly synthesized compounds (**7a-7n**) were tested for anticancer activity against three human breast cancer cell lines including MCF-7, MDA-MB-468 and MDA-MB-231. This analysis was done using MTT assay and we have used 5-fluorouracil (5-FU) as reference drug. Among all the compounds that were screened, four compounds namely **7d**, **7i**, **7k**, and **7n** were displayed superior activity than 5-fluorouracil reference towards three breast cancer cell lines with IC_{50} values ranging from 1.8 µM to 9.7 µM (**Table 1**). To be specific, the compound **7d** has exhibited remarkable anti breast cancer activity against three cell lines MCF-7, MDA-MB-468 and MDA-MB-231 with IC_{50} values 2.9 µM, 1.8 µM and 3.2 µM respectively. Similarly the compound **7k** which has nitro group at 4th position of phenyl ring attached to 1,2,3-triazole unit has shown predominant activity against same cell lines with IC_{50} values 4.5 µM, 3.2 µM and 3.9 µM respectively.

The effect of different substituents on phenyl ring attached to 1,2,3-triazole unit on anticancer activity i.e. structure-activity relationship-SAR was analysed and presented here. For the case of compounds with electron releasing groups, the compound **7d** with methoxy group at 4th position has exhibited greater activity compared to all other compounds and 5-FU against three cell lines. The compound **7e** with two methoxy groups at 3rd and 5th position has exhibited less activity than **7d** but more active than

all other compounds with donating groups. The compounds having methyl substituents **7b** (4-Me) and **7c** (3,5-di-Me) have exhibited greater anticancer activity than the compound **7a** which has no substituent. On the other hand in case of compounds with electron-withdrawing groups on phenyl ring, the compounds **7i** (having two chlorine atoms at 3rd and 5th position) and **7k** (having nitro group at 4th position) have exhibited highest activity than standard 5-fluorouracil against three cell lines. In the case of compounds with one halogen atom the activity was found to be in the order of 4-Br>3-Cl>4-Cl>4-F. The compound **7j** with chlorine atom at 3rd position was shown more activity than compound **7g** with chlorine atom at 4th position. The compound **7l** with nitro group at 3rd position has shown less activity than the compound **7k** with nitro group at 4th position. Further, the compound **7m** were shown good activity compared to the compounds with mono halogen substituent. Finally the compound **7n** with two methoxy groups at 3rd and 5th position and one chlorine atom at 4th position has exhibited significant anticancer activity which is more compared to reference drug. Overall we can say that compounds with electron withdrawing groups have shown more activity than the compounds with electron releasing groups on phenyl ring. Further the compounds **7d**, **7i**, **7k**, and **7n** were displayed very less toxicity (IC_{50} >100 μM) towards normal cell line MCF-10A.

In vitro tyrosine kinase EGFR inhibitory activity

The compounds **7d**, **7i**, **7k**, and **7n** which were shown good in vitro anticancer activity were screened for in vitro tyrosine kinase EGFR inhibitory efficiency using erlotinib as the reference drug.

According to the results which were presented in **Table 2** the compounds, **7d** has displayed predominant inhibitory activity

which was approximately 2.8 times than that of erlotinib with IC_{50} value of 0.15μM. The reference drug erlotinib has shown IC_{50} value of 0.42 μM. Similarly the compound **7k** has exhibited greater inhibition (2 times) than erlotinib with IC_{50} value of 0.21 μM. Further the compounds **7i** and **7n** also shown significant inhibitory activity towards EGFR with IC_{50} values 0.30 μM and 0.35 μM respectively.

Table 1: In vitro anticancer activity of compounds (7a-7n) with IC50 in μM[a].

Entry	R	MCF-7	MDA-MB-468	MDA-MB-231	MCF-10A
7a	H	74.8±1.2	62.5±1.3	75.4±2.1	NT
7b	4-Me	45.2±1.1	48.2±1.5	37.2 ± 1.3	NT
7c	3,5-di-Me	34.8±1.1	37.8±2.1	22.4±1.2	NT
7d	4-OMe	2.9±0.1	1.8±0.1	3.2±0.1	>100
7e	3,5-di-OMe	17.4±1.2	26.1±1.1	16.2±1.1	NT
7f	4-F	62.6±1.6	58.2±1.2	55.4±1.1	NT
7g	4-Cl	48.6±1.4	39.5±1.3	44.7±1.2	NT
7h	4-Br	34.8±1.6	34.6±1.7	45.4±1.1	NT
7i	3,5-di-Cl	9.7±0.1	6.9±0.1	7.7±0.1	>100
7j	3-Cl	42.1±1.2	31.7±1.4	46.8±1.4	NT
7k	4-NO_2	4.5±0.1	3.2±0.1	3.9±0.1	>100
7l	3-NO_2	23.5±0.1	31.1±0.1	43.1±0.1	NT
7m	4-CN	15.7±1.1	17.5±1.2	18.2±1.4	NT
7n	3,5-di-OMe-4-Cl	7.4±0.1	6.3±0.1	8.7±0.1	>100
5FU	-	12.4±0.1	7.8±0.1	11.2±0.1	NT

[a]=Average of triplicates± standard deviation; NT= Not Tested

Table 2. Tyrosine kinase EGFR inhibitory activity.

Compound	IC_{50}(μM)* against EGFR
7d	0.15±0.01
7i	0.30±0.02
7k	0.21±0.01
7n	0.35±0.02
Erlotinib	0.42±0.01

*Average of triplicates± standard deviation

Molecular docking studies

Molecular docking studies were carried out on four 1,2,3-triazole compounds **7d**, **7i**, **7k** and **7n** which displayed greater *in vitro* anticancer activity by taking epidermal growth factor receptor as the target protein (pdb id 4HJO).[34] According to the results which are presented in **Table 3** the compound **7d** having 4-methoxy substituent has exhibited greatest binding energy i.e. -11.04 kcal/mol and formed three hydrogen bonds with LYS721, CYS751 and PHE832 residues having bond lengths 2.25 Å, 1.91 Å and 2.12 Å respectively (**Figure 2** and **Figure 3**). Similarly the compound **7k** also formed three hydrogen bonds with MET769, CYS773 and PHE832 residues having bond lengths 2.36 Å, 2.24 Å and 2.20 Å respectively and it has exhibited second highest binding energy (-10.62 kcal/mol). Further the compound **7i** has exhibited -10.06 kcal/mol, binding energy and it has formed one hydrogen bond with ASN818 residue with bond length 2.48 Å. It also formed π–cation with LYS721 residue. On the other hand the compound **7n** has formed two hydrogen bonds with LYS721 and CYS773 with bond lengths 1.89 Å and 2.25 Å respectively in addition to significant binding energy (-9.75 kcal/mol). Finally, the standard drug, erlotinib also docked with EGFR where it has shown -7.70 kcal/mol, binding energy and 2.28 micro molar, inhibition constant. It also formed one hydrogen bond with THR830 residue with bond length 2.25 Å in addition to π–cation with LYS721 residue.

Table 3. Molecular docking results of compounds (7d, 7i, 7k and 7n) with EGFR (PDB ID-4HJO).

Entry	Binding Energy (kcal/mol)	Inhibition Constant (nM)	No. of hydrogen bonds	Residues involved in hydrogen bonding (bond length in Å)
7d	-11.04	8.13	3	LYS721(2.25), CYS751(1.91), PHE832(2.12)
7i	-10.06	42.58	1	ASN818(2.48)
7k	-10.62	16.30	3	MET769(2.36), CYS773(2.24), PHE832(2.20)
7n	-9.75	70.98	2	LYS721(1.89), CYS773(2.25)
Erlotinib	-7.70	2.28 μM	1	THR830(2.25)

DFT Calculations

Nowadays to support the experimental results the researchers are immensely interested in computational methods. The DFT calculation has been used generally to determine the optimized

structural parameters such as bond lengths and bond angles. Frontier molecular orbitals HOMO – LUMO, Molecular Electrostatic Potential (MEP) and Mulliken atomic charges were calculated for the molecule **7d**.

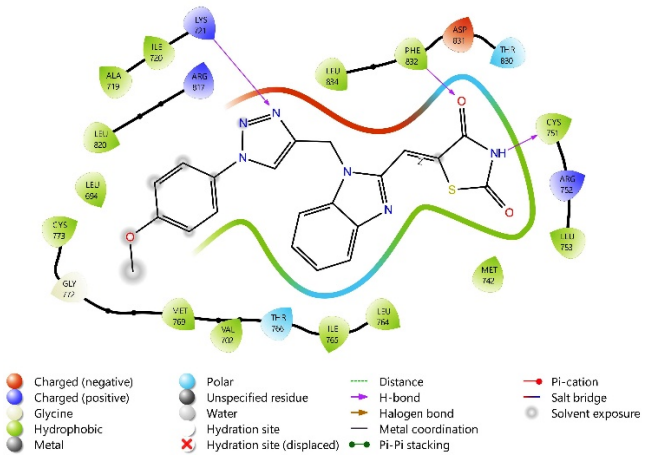

Figure 2: 2D interaction diagram of compound **7d** with EGFR

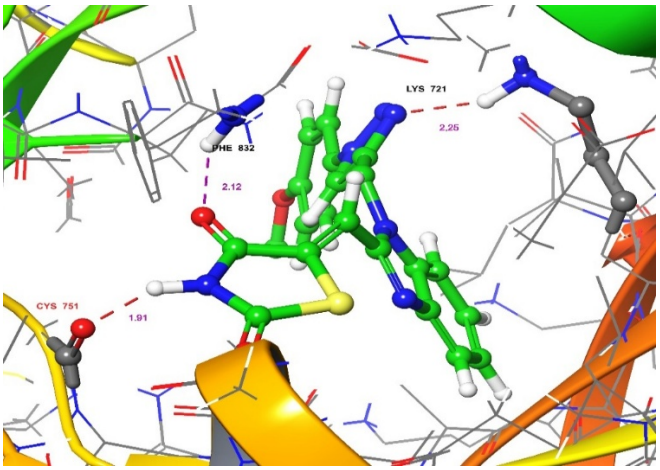

Figure 3: 3D interaction diagram of compound **7d** with EGFR

Molecular geometry

The Molecular structure along with the numbering of atoms of **7d** is shown in **Figure 4**. This molecule has Seventeen C–C bond lengths, ten C–N bond lengths, two N–N bond lengths, two C-S bond lengths and four C–O bond lengths. From the structural data given in ESI (**Table S1)** , it is observed that the various benzene ring C–C bond distance and C–H bond lengths of the **7d** molecule are found. The C7-N12, C17-O23 and C18-O20 possess double bond distance is 1.3389 Å, 1.2433 Å and 1.2229 Å, and C24-O30, C29-N32, N32-C33, C40-O43 and O43-C44 possess single bond distance is 1.382 Å, 1.3673 Å, 1.427 Å, 1.3872 Å, 1.432 Å and1.4545 Å. Moreover, highest bond length C24-C25 is 1.4952 Å on the other hand N21-H22 possess lower bond distance is 1.0095 Å. The maximum value of bond angle was observed between C6-C1-N13 as 132.1533 °.

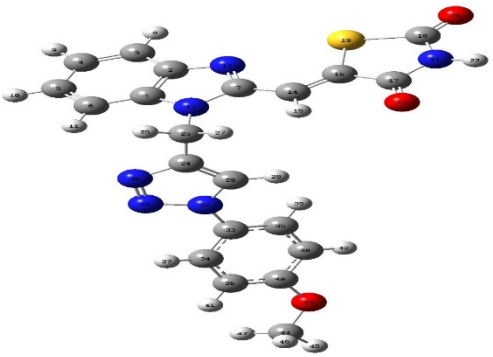

Figure 4. Optimized geometrical structure of **7d** by using DFT calculations.

Molecular electrical potential surface

The calculation of a molecule's charged regions helps to understand molecular interactions and the characteristics of its chemical bonds. The charge distribution within molecules can be visualized in three dimensions using the molecular electrostatic potential surface. This visualization is significant as it illustrates the molecule's size, shape, and the distribution of positive, negative, and neutral electrostatic potentials through color gradients. Therefore, this method[35] can be used to analyze the physicochemical properties of a molecule, including (a) the reactive properties of nucleic acids and their constituent bases, (b) biological recognition processes such as drug-receptor and enzyme-substrate interactions, and (c) chemical carcinogenesis, particularly in relation to polycyclic aromatic hydrocarbons, halogenated olefins, and their epoxides, among others.[36] The different colors in **Figure 5** show different values of the electrostatic potential at the surface of the title compound. The electrostatic potential increases in the order red < orange < yellow < green < blue. The colour code of the maps was found to be in the range of -5.727e-2 a.u (deepest red) to 5.727e-2 a.u. (deepest blue), the red colour suggested that the strongest repulsion (electrophilic attack) and the blue colour indicates the strongest attraction (nucleophilic attack). Regions of negative V(r) are generally related with the lone pair of an electronegative atom. As seen in **Figure 5**, the negative electrostatic potential is present over the oxygen atom of thiazolidine-dione, methoxy and nitrogen atoms of benzimidazole, thiazolidine-dione and triazole while positive electrostatic potential is present over the hydrogen atoms associated with carbon atom. The high allied of the light green colour represents the neutral region between the ends, red and blue.[37] Regions in the molecule could be a suitable information for intermolecular interactions and MEP diagram is also suggested the behavior to approaching protons.

Electronic properties

The Molecular Orbital (MO) analysis of the highest occupied molecular orbital (HOMO) and the lowest unoccupied molecular orbital (LUMO) and their energies (E_{HOMO} and E_{LUMO}) provides insight into the chemical reactivity and stability of a molecule. The spatial distributions of the HOMO and LUMO orbitals of the molecule are shown in **Figure 6**. E_{HOMO} and E_{LUMO} are linked to the electron affinity and ionization energy, which in turn

influence the chemical potential, electronegativity, hardness, softness, and electrophilicity as seen in **Table S2** (ESI). The energy gap between the HOMO and LUMO (ΔE) reflects the charge-transfer interaction within the molecule.[38, 39] A small HOMO-LUMO gap indicates high chemical reactivity, low kinetic stability, and softness, while a larger gap suggests a harder molecule with greater stability. The HOMO-LUMO gap is also associated with electronic excitation from the ground state to the excited state. For compound **7d**, the HOMO-LUMO energy gap is 3.43136 eV.

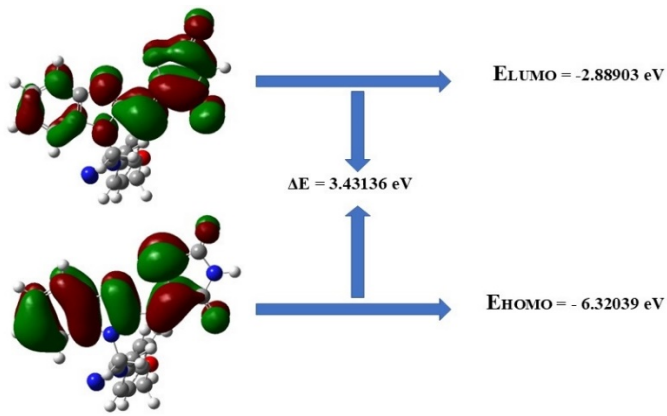

Figure 6: Frontier molecular orbital energy gap of **7d** molecule.

Mulliken atomic charges

These charges play a crucial role in Density Functional Theory (DFT) calculations, particularly in the optimization of molecular geometry, as well as in determining the dipole moment and the electronic structure of the molecule.[40-42] Mulliken atomic charges of **7d** have been computed using the DFT/B3LYP/6- 311G ++ (d, p) basis set and are collected in **Table S3 (ESI)**, where it could be seen that the seven carbon atoms like C7, C17, C18, C24, C29, C33, and C40 possess positive charges and fourteen carbon atoms like C1, C2, C3, C4, C5, C6, C14, C16, C25, C34, C35, C36, C38 and C44 atoms possess negative charges (**Figure 7**). Similar to the Mulliken atomic charges, here, the S19 and N31 possess positive charges and N12, N13, O20, N21, O23, N30, N32 and O43 atoms possess high electronegativity. Besides, the positive charge distribution observed on the all-hydrogen atoms.

In silico pharmacokinetic profile (ADMET)

Asper the literature survey absorption, distribution, metabolism, excretion, and toxicity (ADMET) data has vital importance in the discovery and development of new drug candidates as it helps in predicting a drug's behavior after administration and supports critical decisions regarding whether drug candidates should be advanced, held, or discontinued.[43] Because of this we have evaluated the pharmacokinetic profile of four potent compounds **7d**, **7i**, **7k** and **7n** with the help of pkCSM[44] and SWISSDME.[45] The results were presented in supporting file [**Table S4** (ADME), **Table S4** (Toxicity) and **Table S6** (Drug Likeness)]. All the four compounds have poor water solubility. The Caco2 permeability of the compounds **7d**, **7i**, and **7n** was found positive and that of **7k** was negative. All the four compounds have shown intestinal absorption greater than 87%. The volume of distribution (log L/kg) of all the four compounds was negative and fraction unbound was positive. Similarly all of them were exhibited negative values of CNS permeability (log PS) and blood-brain barrier permeability (log BB). Further all the compounds interacted with cytochrome P450 and inhibited it along with CYP2C19 and CYP2C9. The excretion of the compounds which was measured with log value of ml/min/kg was found to be 0.639, 0.367, 0.345 and 0.463 for the compounds **7d**, **7i**, **7k** and **7n** respectively. In case of toxicity prediction the compounds **7d** and **7k** have shown AMES toxicity and compounds **7d** and **7n** have shown hepato toxicity. Further the compound **7k** has inhibited hERG I and hERG II but remaining three compounds inhibited only hERG II. None of them shown skin permeation. The maximum tolerated dose (human; expressed in log value of mg/kg/day) of the compounds **7d**, **7i**, **7k** and **7n** was 0.082, 0.123, 0.059 and 0.198 respectively.

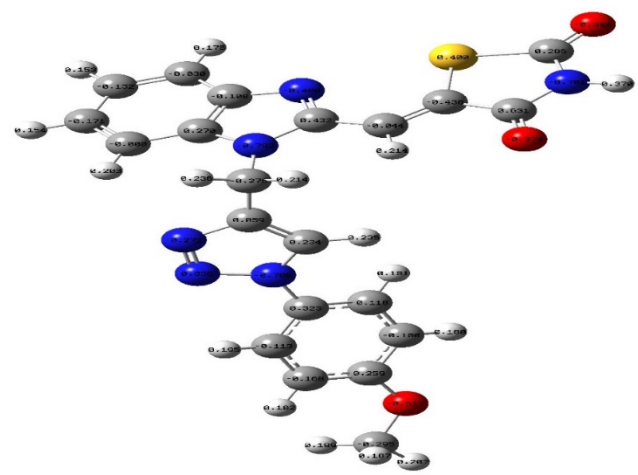

Figure 7: Mulliken atomic charges of **7d** molecule.

The compounds **7d** and **7i** have followed all the rules i.e. Lipinski rule, Ghose rule, Veber rule, Egan rule and Muegge rule without any deviation. But the compound **7k** has followed only Lipinski rule and Ghose rule but not others because of more topological surface area (TPSA). The lipophilicity (Log $P_{o/w}$) of the compounds **7d**, **7i**, **7k** and **7n** was found to be 2.31, 3.31, 1.51, and 2.83 respectively.

EXPERIMENTAL SECTION

Synthesis of 1-(prop-2-yn-1-yl)-1H-benzo[d]imidazole-2-carbaldehyde (3): A mixture of 1*H*-benzo[*d*]imidazole-2-carbaldehyde (**1**) (0.027 mol), K_2CO_3 (0.068 mol) and 3-bromoprop-1-yne (**2**) (0.038 mol) in 25 mL of DMF was stirred at RT for 4 h. The progress of the reaction as analysed by the TLC, excess of ice cold water was then added to the reaction mixture. The resulting crude product was filtered and purified by 60-120 mesh size silica gel column chromatography using (3:7) ethyl acetate/hexane eluent.

1-(prop-2-yn-1-yl)-1*H*-benzo[*d*]imidazole-2-carbaldehyde (**3**): Colorless solid; Yield 76%; MP: 187-189 °C; ^{1}H NMR (400 MHz, DMSO-d_6) δ 2.33 (s, 1H), 4.71 (s, 2H), 7.34 (t, *J* = 7.6 Hz, 1H), 7.45 (t, *J* = 7.6 Hz 1H), 7.78-7.83 (m, 2H), 9.83 (s, 1H) ppm;

Synthesis of (Z)-5-((1-(prop-2-yn-1-yl)-1H-benzo[d]imidazol-2-yl)methylene)thiazolidine-2,4-dione (5): A mixture of intermediate **3** (0.0195 mol), thiazolidine-2,4-dione (**4**) (0.0195 mol) and piperidine (0.00195 mol) in EtOH (30 mL) was refluxed for 24 h. Later the reaction mixture was cooled for overnight and resulting solid was filtered and purified by recrystallization process using EtOH solvent.

1-(prop-2-yn-1-yl)-1*H*-benzo[*d*]imidazole-2-carbaldehyde (**5**): Colorless solid; Yield 65%; MP: 240-242 ºC; ^{1}H NMR (400 MHz, DMSO-d_6) δ 2.31(s, 1H), 4.73 (s, 2H), 7.34 (t, *J* = 7.6 Hz, 1H), 7.46 (t, *J* = 7.6 Hz 1H), 7.70 (s, 1H), 7.81-7.86 (m, 2H), 12.42 (br s, 1H, NH) ppm.

General procedure for the synthesis of benzimidazole-thiazolidine-2,4-dione-1,2,3-triazole hybrids (7a-7n). To a mixture of intermediate **5** (0.5 mmol) and aryl azides (**6a–6n**) (1.0 mmol) in THF (15 mL) was added CuI (0.05 mmol) and resulting reaction mixture was allowed to stirring at RT for 15 h. Later, the reaction was extracted twice with ethyl acetate (20 mL). The combined organic layer dried over anhydrous Na_2SO_4 and evaporated under vacuum. Finally, the crude products were subjected to purification by 60-120 mesh size silica gel column chromatography using (1:1) ethyl acetate/hexane eluent.

(Z)-5-((1-((1-phenyl-1*H*-1,2,3-triazol-4-yl)methyl)-1*H*-benzo[*d*]imidazol-2-yl)methylene) thiazolidine-2,4-dione (7a): Colorless solid; Yield 76%; MP: 284-286 ºC; ^{1}H NMR (400 MHz, DMSO-d_6) δ 4.96 (s, 2H), 7.36 (t, *J* = 7.6 Hz, 1H), 7.43-7.50 (m, 4H), 7.70-7.75 (m, 3H), 7.81-7.86 (m, 2H), 8.42 (s, 1H), 12.44 (br s, 1H, NH) ppm; ^{13}C NMR (100 MHz, DMSO-d_6) δ 48.1, 114.8, 115.6, 118.1, 120.3, 121.8 (2c), 123.1, 123.7, 124.6, 128.1, 129.8 (2c), 137.6, 138.7, 140.5, 141.3, 151.3, 163.1, 168.9 ppm; MS (ESI): m/z = 403 [M+H]$^+$; CHN analysis for $C_{20}H_{14}N_6O_2S$; Calculated (%): C, 59.69; H, 3.51; N, 20.88; Found (%): C, 59.66; H, 3.54; N, 20.90.

(Z)-5-((1-((1-(p-tolyl)-1H-1,2,3-triazol-4-yl)methyl)-1H-benzo[d]imidazol-2-yl)methylene)thiazolidine-2,4-dione (7b): Cream solid; Yield 76%; MP: 288-290 ºC; ^{1}H NMR (400 MHz, DMSO-d_6) δ 2.38 (s, 3H), 4.94 (s, 2H), 7.32-7.39 (m, 3H), 7.44 (t, *J* = 7.6 Hz, 1H), 7.69 (s, 1H), 7.80-7.87 (m, 4H), 8.41 (s, 1H), 12.46 (br s, 1H, NH) ppm; ^{13}C NMR (100 MHz, DMSO-d_6) δ 21.5, 47.9, 114.8, 115.5, 118.2, 120.2, 123.1, 123.6, 124.7, 125.2 (2c), 129.3 (2c), 137.3, 138.7, 139.2, 140.4, 141.2, 151.2, 162.7, 168.6 ppm; MS (ESI): m/z = 439 [M+Na]$^+$; CHN analysis for $C_{21}H_{16}N_6O_2S$; Calculated (%): C, 60.57; H, 3.87; N, 20.18; Found (%): C, 60.54; H, 3.85; N, 20.22;.

(Z)-5-((1-((1-(3,5-dimethylphenyl)-1H-1,2,3-triazol-4-yl)methyl)-1H-benzo[d]imidazol-2-yl)methylene)thiazolidine-2,4-dione (7c): Cream solid; Yield 72%; MP: 291-293 ºC; ^{1}H NMR (400 MHz, DMSO-d_6) δ 2.42 (s, 6H), 4.96 (s, 2H), 7.15 (s, 1H), 7.36 (t, *J* = 7.6 Hz, 1H), 7.46 (t, *J* = 7.6 Hz, 1H), 7.52 (s, 2H), 7.71 (s, 1H), 7.80-7.85 (m, 2H), 8.44 (s, 1H), 12.45 (br s, 1H, NH) ppm; ^{13}C NMR (100 MHz, DMSO-d_6) δ 21.9 (2c), 48.2, 114.9, 115.6, 118.3, 120.3, 123.2, 123.8, 124.6, 125.9 (2c), 127.6, 138.7, 138.2, 140.1 (2c), 140.6, 141.3, 151.3, 163.1, 168.7 ppm; MS (ESI): m/z = 431 [M+H]$^+$; CHN analysis for $C_{22}H_{18}N_6O_2S$; Calculated (%): C, 61.38; H, 4.21; N, 19.52; Found (%): C, 61.35; H, 4.23; N, 19.50.

(Z)-5-((1-((1-(4-methoxyphenyl)-1H-1,2,3-triazol-4-yl)methyl)-1H-benzo[d]imidazol-2-yl)methylene)thiazolidine-2,4-dione (7d): Colorless solid; Yield 73%; MP: 292-294 ºC; ^{1}H NMR (400 MHz, DMSO-d_6) δ 3.87 (s, 3H), 4.95 (s, 2H), 6.94 (d, *J* = 7.5 Hz, 2H), 7.35 (t, *J* = 7.6 Hz, 1H), 7.44 (t, *J* = 7.6 Hz, 1H), 7.62 (d, *J* = 7.7 Hz, 2H), 7.72 (s, 1H), 7.79-7.84 (m, 2H), 8.44 (s, 1H), 12.43 (br s, 1H, NH) ppm; ^{13}C NMR (100 MHz, DMSO-d_6) δ 48.1, 56.4, 114.2 (2c), 114.8, 115.7, 118.2, 120.3, 123.2, 123.6, 124.5, 125.1 (2c), 132.1, 138.6, 140.4, 141.2, 151.1, 159.1, 162.8, 168.6 ppm; MS (ESI): m/z = 433 [M+H]$^+$; CHN analysis for $C_{21}H_{16}N_6O_3S$; Calculated (%): C, 58.32; H, 3.73; N, 19.43; Found (%): C, 58.30; H, 3.76; N, 19.44.

(Z)-5-((1-((1-(3,5-dimethoxylphenyl)-1H-1,2,3-triazol-4-yl)methyl)-1H-benzo[d]imidazol-2-yl)methylene)thiazolidine-2,4-dione (7e): Grey solid; Yield 68%; MP: 297-299 ºC; ^{1}H NMR (400 MHz, DMSO-d_6) δ 3.89 (s, 6H), 4.94 (s, 2H), 6.73 (s, 1H), 7.18 (s, 2H), 7.35 (t, *J* = 7.6 Hz, 1H), 7.45 (t, *J* = 7.6 Hz, 1H), 7.69 (s, 1H), 7.81-7.86 (m, 2H), 8.45 (s, 1H), 12.42 (br s, 1H, NH) ppm; ^{13}C NMR (100 MHz, DMSO-d_6) δ 47.8, 56.8 (2c), 98.3, 99.7 (2c), 114.6, 115.7, 118.3, 120.4, 123.3, 123.8, 124.6, 138.7, 140.6, 141.4, 141.8, 151.2, 160.8 (2c), 163.1, 168.9 ppm; MS (ESI): m/z = 463 [M+H]$^+$; CHN analysis for $C_{22}H_{18}N_6O_4S$; Calculated (%): C, 57.14; H, 3.92; N, 18.17; Found (%): C, 57.18; H, 3.90; N, 18.19.

(Z)-5-((1-((1-(4-fluorophenyl)-1H-1,2,3-triazol-4-yl)methyl)-1H-benzo[d]imidazol-2-yl)methylene)thiazolidine-2,4-dione (7f): Light solid; Yield 82%; MP: 285-287 ºC; ^{1}H NMR (400 MHz, DMSO-d_6) δ 4.97 (s, 2H), 7.16 (d, J = 7.3 Hz, 2H), 7.37 (t, *J* = 7.6 Hz, 1H), 7.46 (t, *J* = 7.6 Hz, 1H), 7.55 (d, *J* = 7.3 Hz, 2H), 7.73 (s, 1H), 7.80-7.85 (m, 2H), 8.48 (s, 1H), 12.45 (br s, 1H, NH) ppm; ^{13}C NMR (100 MHz, DMSO-d_6) δ 48.3, 114.9, 115.9, 117.5 (2c), 118.2, 120.3, 123.2, 123.9, 124.3 (2c), 124.8, 134.2, 138.8, 140.7, 141.4, 151.4, 161.1, 163.2, 169.2 ppm; MS (ESI): m/z = 421 [M+H]$^+$; CHN analysis for $C_{20}H_{13}FN_6O_2S$; Calculated (%): C, 57.14; H, 3.12; N, 19.99; Found (%): C, 57.16; H, 3.15; N, 19.97.

(Z)-5-((1-((1-(4-chlorophenyl)-1H-1,2,3-triazol-4-yl)methyl)-1H-benzo[d]imidazol-2-yl)methylene)thiazolidine-2,4-dione (7g): Colorless solid; Yield 80%; MP: 287-289 ºC; ^{1}H NMR (400 MHz, DMSO-d_6) δ 4.95 (s, 2H), 7.33-7.40 (m, 3H), 7.46 (t, *J* = 7.6 Hz, 1H), 7.71 (s, 1H), 7.76 (d, *J* = 7.4 Hz, 2H), 7.82-7.87 (m, 2H), 8.46 (s, 1H), 12.43 (br s, 1H, NH) ppm; ^{13}C NMR (100 MHz, DMSO-d_6) δ 48.1, 114.8, 115.7, 118.2, 120.3, 122.6 (2c), 123.1, 123.7, 124.7, 129.7 (2c), 134.1, 137.2, 138.6, 140.5, 141.2, 151.2, 163.1, 168.9 ppm; MS (ESI): m/z = 437 [M+H]$^+$; CHN analysis for $C_{20}H_{13}ClN_6O_2S$; Calculated (%): C, 54.99; H, 3.00; N, 19.24; Found (%): C, 54.96; H, 3.02; N, 19.25.

(Z)-5-((1-((1-(4-bromophenyl)-1*H*-1,2,3-triazol-4-yl)methyl)-1*H*-benzo[*d*]imidazol-2-yl)methylene)thiazolidine-2,4-dione (7h): Light orange solid; Yield 77%; MP: >300 ºC; ^{1}H NMR (400 MHz, DMSO-d_6) δ 4.96 (s, 2H), 7.36 (t, *J* = 7.6 Hz, 1H), 7.42-7.49 (m, 3H), 7.72 (s, 1H), 7.81-7.89 (m, 4H), 8.44 (s, 1H), 12.44 (br s, 1H, NH) ppm; ^{13}C NMR (100 MHz, DMSO-d_6) δ 48.2, 114.7, 115.6, 118.3, 120.4, 121.4, 122.1 (2c), 123.1, 123.6, 124.5, 132.5 (2c), 136.1, 138.8, 140.7, 141.3, 151.4, 163.2, 169.1 ppm; MS (ESI): m/z = 482 [M+H]$^+$; CHN analysis for

$C_{20}H_{13}BrN_6O_2S$: Calculated (%): C, 49.91; H, 2.72; N, 17.46; Found (%): C, 49.89; H, 2.52; N, 17.48.

(Z)-5-((1-((1-(3,5-dichlorophenyl)-1*H*-1,2,3-triazol-4-yl)methyl)-1*H*-benzo[*d*]imidazol-2-yl)methylene)thiazolidine-2,4-dione (7i): Cream solid; Yield 82%; MP: 293-295 ºC; ^{1}H NMR (400 MHz, DMSO-d$_6$) δ 4.95 (s, 2H), 7.36 (t, *J* = 7.6 Hz, 1H), 7.45 (t, *J* = 7.6 Hz, 1H), 7.55 (s, 1H), 7.71 (s, 1H), 7.78-7.87 (m, 4H), 8.47 (s, 1H), 12.42 (br s, 1H, NH) ppm; ^{13}C NMR (100 MHz, DMSO-d$_6$) δ 48.1, 114.8, 115.5, 118.2, 119.1 (2c), 120.3, 123.2, 123.7, 124.7, 125.3, 136.1 (2c), 138.9, 139.7, 140.5, 141.2, 151.3, 162.9, 168.8 ppm; MS (ESI): m/z = 472 [M+H]$^+$; CHN analysis for $C_{20}H_{12}Cl_2N_6O_2S$; Calculated (%): C, 50.97; H, 2.57; N, 17.83; Found (%): C, 50.99; H, 2.55; N, 17.86.

(Z)-5-((1-((1-(3-chlorophenyl)-1*H*-1,2,3-triazol-4-yl)methyl)-1*H*-benzo[*d*]imidazol-2-yl)methylene)thiazolidine-2,4-dione (7j): Colorless solid; Yield 78%; MP: 288-290 ºC; ^{1}H NMR (400 MHz, DMSO-d$_6$) δ 4.94 (s, 2H), 7.09-7.14 (m, 2H), 7.32-7.39 (m, 2H), 7.46 (t, *J* = 7.6 Hz, 1H), 7.63 (s, 1H), 7.73 (s, 1H), 7.80-7.85 (m, 2H), 8.49 (s, 1H), 12.44 (br s, 1H, NH) ppm; ^{13}C NMR (100 MHz, DMSO-d$_6$) δ 47.9, 114.7, 115.6, 118.3, 119.1, 120.4, 121.8, 123.1, 123.9, 124.6, 126.3, 131.1, 134.5, 138.8, 139.9, 140.6, 141.4, 151.2, 163.2, 169.1 ppm; MS (ESI): m/z = 437 [M+H]$^+$; CHN analysis for $C_{20}H_{13}ClN_6O_2S$; Calculated (%): C, 54.99; H, 3.00; N, 19.24; Found (%): C, 54.95; H, 3.02; N, 19.27.

(Z)-5-((1-((1-(4-nitrophenyl)-1*H*-1,2,3-triazol-4-yl)methyl)-1*H*-benzo[*d*]imidazol-2-yl)methylene)thiazolidine-2,4-dione (7k): Light yellow solid; Yield 82%; MP: 294-296 ºC; ^{1}H NMR (400 MHz, DMSO-d$_6$) δ 4.98 (s, 2H), 7.36 (t, *J* = 7.6 Hz, 1H), 7.47 (t, *J* = 7.6 Hz, 1H), 7.72 (s, 1H), 7.81-7.88 (m, 4H), 8.30 (d, J = 7.2 Hz, 2H), 8.51 (s, 1H), 12.45 (br s, 1H, NH) ppm; ^{13}C NMR (100 MHz, DMSO-d$_6$) δ 48.3, 114.9, 115.8, 118.3, 120.5, 122.8 (2c), 123.2, 124.1, 124.7, 126.5 (2c), 138.9, 140.7, 141.5, 142.8, 148.4, 151.4, 163.5, 169.4 ppm; MS (ESI): m/z = 470 [M+Na]$^+$; CHN analysis for $C_{20}H_{13}N_7O_4S$; Calculated (%): C, 53.69; H, 2.93; N, 21.91; Found (%): C, 53.72; H, 2.95; N, 21.90.

(Z)-5-((1-((1-(3-nitrophenyl)-1*H*-1,2,3-triazol-4-yl)methyl)-1*H*-benzo[*d*]imidazol-2-yl)methylene)thiazolidine-2,4-dione (7l): Yellow solid; Yield 85%; MP: 295-297 ºC; ^{1}H NMR (400 MHz, DMSO-d$_6$) δ 4.95 (s, 2H), 7.35 (t, *J* = 7.6 Hz, 1H), 7.42-7.49 (m, 2H), 7.71 (s, 1H), 7.68-7.75 (m, 2H), 7.80-7.85 (m, 2H), 8.53 (s, 1H), 8.82 (s, 1H), 12.43 (br s, 1H, NH) ppm; ^{13}C NMR (100 MHz, DMSO-d$_6$) δ 47.9, 114.8, 115.7, 118.2, 120.3, 120.9, 122.1, 123.3, 124.2, 124.8, 128.6, 131.7, 138.1, 138.8, 140.6, 141.3, 148.1, 151.2, 163.1, 168.9 ppm; MS (ESI): m/z = 448 [M+H]$^+$; CHN analysis for $C_{20}H_{13}N_7O_4S$; Calculated (%): C, 53.69; H, 2.93; N, 21.91; Found (%): C, 53.67; H, 2.95; N, 21.88.

(Z)-4-(4-((2-((2,4-dioxothiazolidin-5-ylidene)methyl)-1*H*-benzo[*d*]imidazol-1-yl)methyl)-1*H*-1,2,3-triazol-1-yl)benzonitrile (7m): Orange solid; Yield 80%; MP: 286-288 ºC; ^{1}H NMR (400 MHz, DMSO-d$_6$) δ 4.97 (s, 2H), 7.36 (t, *J* = 7.6 Hz, 1H), 7.46 (t, *J* = 7.6 Hz, 1H), 7.52 (d, *J* = 7.6 Hz, 2H), 7.72 (s, 1H), 7.80-7.85 (m, 2H), 7.90 (d, *J* = 7.6 Hz, 2H), 8.49 (s, 1H), 12.45 (br s, 1H, NH) ppm; ^{13}C NMR (100 MHz, DMSO-d$_6$) δ 48.2, 114.7, 115.6, 117.6, 118.3, 119.6, 120.2, 123.2, 123.9, 124.7, 125.7 (2c), 126.4 (2c), 138.6, 139.8, 140.5, 141.4, 151.3, 162.8, 168.8 ppm; MS (ESI): m/z = 428 [M+H]$^+$; CHN analysis for $C_{21}H_{13}N_7O_2S$; Calculated (%): C, 59.01; H, 3.07; N, 22.94; Found (%): C, 59.04; H, 3.04; N, 22.98.

(Z)-5-((1-((1-(4-chloro-3,5-dimethoxyphenyl)-1*H*-1,2,3-triazol-4-yl)methyl)-1*H*-benzo[*d*]imidazol-2-yl)methylene)thiazolidine-2,4-dione (7n): Colorless solid; Yield 72%; MP: 297-299 ºC; ^{1}H NMR (400 MHz, DMSO-d$_6$) δ 3.90 (s, 6H), 4.94 (s, 2H), 6.77 (s, 2H), 7.35 (t, *J* = 7.6 Hz, 1H), 7.44 (t, *J* = 7.6 Hz, 1H), 7.70 (s, 1H), 7.81-7.86 (m, 2H), 8.43 (s, 1H), 12.42 (br s, 1H, NH) ppm; ^{13}C NMR (100 MHz, DMSO-d$_6$) δ 47.8, 56.9 (2c), 106.5 (2c), 114.8, 115.7, 118.2, 118.9, 120.4, 123.1, 123.6, 124.5, 138.5, 139.2, 140.4, 141.5, 151.2, 153.7 (2c), 163.3, 169.2 ppm; MS (ESI): m/z = 497 [M+H]$^+$; CHN analysis for $C_{22}H_{17}ClN_6O_4S$; Calculated (%): C, 53.18; H, 3.45; N, 16.91; Found (%): C, 53.20; H, 3.48; N, 16.89.

Conclusion

Here we have followed well known copper (I) catalysed azide alkyne cycloaddition to synthesize benzimidazole- thiazolidine-2,4-dione -1,2,3-triazole conjugates (**7a-7n**). In vitro anticancer activity against three human breast cancer cell lines like MCF-7, MDA-MB-468 and MDA-MB-231 revealed that four compounds **7d**, **7i**, **7k**, and **7n** have shown superior activity than 5-fluorouracil. In vitro tyrosine kinase EGFR inhibition assay given that same four compounds **7d**, **7i**, **7k**, and **7n** have displayed more inhibition than erlotinib. Molecular docking studies were carried out on EGFR protein shown that compound **7d** has exhibited significant binding energy i.e. -11.04 kcal/mol compared to erlotinib. Further the molecule **7d** was characterized by using density functional theory (DFT) with B3LYP/6–311++ G (d, p) basis set.

Acknowledgements

The authors are thankful to the Department of Chemistry, Chaitanya (Deemed to be University) for providing lab facilities.

Conflict of Interest Statement

The authors have no conflict of interest (financial or academic) for this work.

References

1. B.S. Chhikara, K. Parang. Global Cancer Statistics 2022: the trends projection analysis. *Chem. Biol. Lett.* **2023**, 10 (1), 451.
2. M. Abotaleb, P. Kubatka, M. Caprnda et.al. Chemotherapeutic agents for the treatment of metastatic breast cancer: An update. *Biomed. Pharmacother*. **2018**, 101, 458-477.
3. A. Remesh. Toxicities of anticancer drugs and its management. *Int. J. Basic Clin. Pharmacol*. **2012**, 1(2), 2319-2003.
4. X. Liang, Q. Wu, S. Luan, Z. Yin, C. He, L. Yin, Y. Zou, Z. Yuan, L. Li, X. Song, M. He. A comprehensive review of topoisomerase inhibitors as anticancer agents in the past decade. *Eur. J. Med. Chem*. **2019**, 171, 129-168.
5. Y.J. Guo, W.W. Pan, S.B. Liu, Z.F. Shen, Y. Xu, L.L. Hu. ERK/MAPK signalling pathway and tumorigenesis. *Exp. Ther. Med*. **2020**, 19(3), 1997-2007.
6. E. Zwick, J. Bange, A. Ullrich. Receptor tyrosine kinase signalling as a target for cancer intervention strategies. Endocrine-related cancer. **2001**, 8(3), 161-173.
7. L. Huang, L. Fu. Mechanisms of resistance to EGFR tyrosine kinase inhibitors. *Acta Pharm Sin B*. **2015**, 5(5), 390-401.

8. C. Yewale, D. Baradia, I. Vhora, S. Patil, A. Misra. Epidermal growth factor receptor targeting in cancer: a review of trends and strategies. *Biomaterials*. **2013**, 34(34), 8690-8707.
9. F.A. Mohamed, H.A. Gomaa, O.M. Hendawy, A.T. Ali, H.S. Farghaly, A.M. Gouda, A.H. Abdelazeem, M.H. Abdelrahman, L. Trembleau, B.G. Youssif. Design, synthesis, and biological evaluation of novel EGFR inhibitors containing 5-chloro-3-hydroxymethyl-indole-2-carboxamide scaffold with apoptotic antiproliferative activity. *Bioorg. Chem*. **2021**, 112, 104960.
10. M.J. Akhtar, A.A. Khan, Z. Ali, R.P. Dewangan, M.d. Rafi, M.Q. Hassan, M.S. Akhtar, A.A. Siddiqui, S. Partap, S. Pasha, M.S. Yar. Synthesis of stable benzimidazole derivatives bearing pyrazole as anticancer and EGFR receptor inhibitors. *Bioorg. Chem*. **2018**, 78, 158–169.
11. M. Gaba, S. Singh, C. Mohan. Benzimidazole: An emerging scaffold for analgesic and anti-inflammatory agents. *Eur. J. Med. Chem*. **2014**, 76, 494-505.
12. N. Shrivastava, M.J. Naim, M.J. Alam, F. Nawaz, S. Ahmed, O. Alam. Benzimidazole scaffold as anticancer agent: synthetic approaches and structure–activity relationship. *Arch. Pharm. Chem. Life Sci*. **2017**, 350(6), e201700040.
13. H. Zhang. Osimertinib making a breakthrough in lung cancer targeted therapy. *Onco Targets Ther*. **2016**, 9, 5489–5493.
14. D. Singh, M. Piplani, H. Kharkwal, S. Murugesan, Y. Singh, A. Aggarwal, S. Chander. Anticancer Potential of Compounds Bearing Thiazolidin-4-one Scaffold: Comprehensive Review. *Pharmacophore*. **2023**, 14(1), 56-70.
15. D.S. Bhagat, P.A. Chawla, W.B. Gurnule, S.K. Shejul, G.S. Bumbrah. An insight into synthesis and anticancer potential of thiazole and 4-thiazolidinone containing motifs. *Curr. Org. Chem*. **2021**, 25(7), 819-841.
16. P. Roszczenko, S. Holota, O.K. Szewczyk, R. Dudchak, K. Bielawski, A. Bielawska, R. Lesyk. 4-Thiazolidinone-Bearing Hybrid Molecules in Anticancer Drug Design. *Int. J. Mol. Sci.* **2022**, 23, 13135.
17. B. Saritha, B.B.V. Sailaja. New molecular hybrids containing benzimidazole, thiazolidine-2, 4-dione and 1, 2, 4-oxadiazole as EGFR directing cytotoxic agents. *Tetrahedron*. **2022**, 124, 132991.
18. T. Shreedhar Reddy, S. Rai, S.K. Koppula. Synthesis of 4-azaindole-thiazolidine-2, 4-dione coupled 1, 2, 3-triazoles as EGFR directing anticancer agents. *Polycycl Aromat Comp*. **2024**, 44(8), 5009-5021.
19. R. Kaushik, M. Chand, S.C. Jain. Synthesis and antibacterial evaluation of nitrogen containing novel heterocyclic chalcones. *Synth. Commun*. **2018**, 48, 1308–1315.
20. B. Banerji, K. Chandrasekhar, K. Sreenath, S. Roy, S. Nag, K.D. Saha. Synthesis of triazole-substituted quinazoline hybrids for anticancer activity and a lead compound as the EGFR blocker and ROS inducer agent. *ACS omega*. **2018**, 3(11), 16134-16142.
21. D. Dheer, V. Singh, R. Shankar, Medicinal attributes of 1,2,3-triazoles: Current developments, *Bioorg. Chem*. **2017**, 71, 30–54.
22. R.S. Keri, S.A. Patil, S. Budagumpi, B.M. Nagaraja. Triazole: A Promising Antitubercular Agent, *Chem. Biol. Drug Des*. **2015**, 86, 410–423.
23. N.M. Reddy, R. Vadluri, J. Arasan, et al. Design and synthesis of new Nilutamide-1,2,3-triazole derivatives as in vitro Anticancer agents. *Chem. Biol. Lett.* **2022**, 9 (4), 405.
24. X.M. Peng, G.X. Cai, C.H. Zhou. Recent developments in azole compounds as antibacterial and antifungal agents. *Curr. Top. Med. Chem*. **2013**, 13, 1963–2010.
25. L.R. Peyton, S. Gallagher, M. Hashemzadeh. Triazole antifungals: a review. *Drugs today*. **2015**, 51, 705–718.
26. M.R. Aouad, M.M. Mayaba, A. Naqvi, S.K. Bardaweel, F.F. Al-Blewi, M., N. Rezki. Design, synthesis, in silico and in vitro antimicrobial screenings of novel 1,2,4-triazoles carrying 1,2,3-triazole scaffold with lipophilic side chain tether. *Chem Cent J*. **2017**, 11, 117-117.
27. A. Mamidala, K. Bokkala, N.S. Thirukovela, N. Sirassu, S. Bandari, S.K. Nukala. Synthesis of Quinoline-Morpholine- Coupled 1, 2, 3- Triazole Hybrids as In vitro EGFR inhibitors. *ChemistrySelect*. **2022**, 7(47), e202203763.
28. A. Mamidala, N.S. Thirukovela, A.K. Bapuram, K. Bokkala, S.K. Nukala. Synthesis of Some New Barbituric Acid Linked Quinoline-1, 2, 3-triazole Hybrids as Dual EGFR/VEGFR-2 Inhibitors. *Russ. J. Gen. Chem*. **2024**, 94(6), 1399-1411.
29. M. Kumar, S.K. Nukala, N.S. Thirukovela, R. Sreerama, P. Kamarajugadda, S. Narsimha. Ramachary-Bressy-Wang [3+ 2] cycloaddition reaction: Synthesis of fully decorated 1, 2, 3-triazoles as potent anticancer and EGFR inhibitors. *J. Mol. Struct*. **2022**, 1262, 132975.
30. R. Samala, S. Kumar Nukala, N. Swamy Thirukovela, V. Reddy Nagavelli, S. Narsimha. Cu (I)-Catalyzed One- Pot Synthesis of [1, 2, 3] Triazolo [5, 1-a] isoquinolin- 6 (5H)- one Derivatives as EGFR-Targeting Anticancer Agents. *ChemistrySelect*. **2022**, 7(43), e202203388.
31. E. Ramya Sucharitha, S. Kumar Nukala, N. Swamy Thirukovela, R. Palabindela, R. Sreerama, S. Narsimha. Synthesis and Biological Evaluation of Benzo [d] thiazolyl-Sulfonyl- Benzo [4, 5] isothiazolo [2, 3-c][1, 2, 3] triazole Derivatives as EGFR Targeting Anticancer Agents. *ChemistrySelect*. **2023**, 8(6), e202204256.
32. A.V. Junior, A. Danuello, V. D. S. Bolzani, E. J. Barreiro, C. A. M. Fraga. Molecular Hybridization: A Useful Tool in the Design of New Drug Prototypes. *Curr. Med. Chem*. **2007**, 14, 1829–1852.
33. L. K. Gediya, V. C. Njar. Promise and challenges in drug discovery and development of hybrid anticancer drugs. *Expert Opin. Drug. Discov*. **2009**, 4, 1099–1111.
34. J.H. Park, Y. Liu, M.A. Lemmon, R. Radhakrishnan. Erlotinib binds both inactive and active conformations of the EGFR tyrosine kinase domain. *Biochem. J*. **2012**, 448, 417-423.
35. J.S. Murry, K. Sen. Molecular electrostatic potential concepts and applications. *Theor. Comput. Chem*. **1996**, 3, 1–665.
36. P. Politzer, P.R. Laurence, K. Jayasuriya. Molecular electrostatic potentials: an effective tool for the elucidation of biochemical phenomena, *Environ. Health Perspect*. **1985**, 61, 191–202.
37. Y.B. Shankar Rao, M.V.S. Prasad, N. Udaya Sri, V. Veeraiah. Vibrational (FTIR, FT-Raman) and UV visible spectroscopic studies, HOMOeLUMO, NBO, NLO and MEP analysis of Benzyl (imino (1Hpyrazol-1-yl) methyl) carbamate using DFT calculations. *J. Mol. Struct*. **2016**, 1108, 567–582.
38. R.G. Pearson. Absolute electronegativity and hardness correlated with molecular orbital theory, *Proc. Natl. Acad. Sci*. **1986**, 83, 8440–8441.
39. A. Abdel majid, S.Moamen Adam, T.Sharshar Refat, Z.K. Heiba. Synthesis and characterization of highly conductive charge-transfer complexes using positron annihilation spectroscopy. *Spectrochim. Acta A*. **2012**, 95, 458–477.
40. M.M.C. Ferreira, E. Suto. Atomic polar tensor transferability and atomic charges in the fluoromethane series CHxF4-x. *J. Phys. Chem*. **1992**, 96, 8844–8849.
41. A.D. Becke. Density-functional thermochemistry. III. The role of exact exchange. *J. Chem. Phys*. **1993**, 98 (7), 5648–5652.
42. Lee, W. Yang, R.G. Parr. Development of the Colic-Salvetti correlationenergy formula into a functional of the electron density. *Phys. Rev. B*. **1998**, 37 (2), 785–789.
43. D. Zhang, G. Luo, X. Ding, C. Lu. Preclinical experimental models of drug metabolism and disposition in drug discovery and development. *Acta Pharmaceutica Sinica B*. **2012**, 2 (6), 549-561.
44. Pires DEV, Blundell TL, Ascher DB. pkCSM: Predicting small-molecule pharmacokinetic and toxicity properties using graph-based signatures. *J Med Chem*. **2015**, 58(9), 4066–4072.
45. Daina, O. Michielin, V. Zoete. SwissADME: A free web tool to evaluate pharmacokinetics, drug-likeness and medicinal chemistry friendliness of small molecules.